Contents lists available at ScienceDirect

Journal of Crystal Growth

journal homepage: www.elsevier.com/locate/jcrysgro

Nucleation and coalescence of tungsten disulfide layers grown by metalorganic chemical vapor deposition

Haonan Tang [a], Sergej Pasko [a], Simonas Krotkus [a], Thorsten Anders [a], Cornelia Wockel [a], Jan Mischke [a], Xiaochen Wang [b], Ben Conran [b], Clifford McAleese [b], Ken Teo [b], Sreetama Banerjee [c], Henry Medina Silva [c], Pierre Morin [c], Inge Asselberghs [c], Amir Ghiami [d], Annika Grundmann [d], Songyao Tang [d], Hleb Fiadziushkin [d], Holger Kalisch [d], Andrei Vescan [d], Salim El Kazzi [e], Alain Marty [f], Djordje Dosenovic [f], Hanako Okuno [f], Lucie Le Van-Jodin [g], Michael Heuken [a],[d],*

[a] *AIXTRON SE, Dornkaulstraße 2, 52134 Herzogenrath, Germany*
[b] *AIXTRON Ltd, Anderson Road, Buckingway Business Park, Cambridge CB24 4FQ, UK*
[c] *imec, Kapeldreef 75, 3001 Leuven, Belgium*
[d] *Compound Semiconductor Technology, RWTH Aachen University, 52074 Aachen, Germany*
[e] *Applied Materials-NUS Advanced Materials Corporate Lab, 5 Engineering Drive 1, 117608 Singapore, Singapore*
[f] *University Grenoble Alpes, CEA, CNRS, IRIG-MEM/Spintec, F-38000 Grenoble, France*
[g] *University Grenoble Alpes, CEA, Leti, F-38000 Grenoble, France*

ARTICLE INFO

ABSTRACT

The nucleation of tungsten disulfide WS_2 crystallites and coalescence behaviour of monolayer WS_2 films grown on C-plane sapphire have been studied in a commercial AIXTRON close coupled showerhead metalorganic chemical vapor deposition (MOCVD) reactor using tungsten hexacarbonyl and di-*tert*-butyl sulfide as precursors. The influence of sapphire substrates offcut (both orientation and angle), as well as the substrate annealing conditions and growth temperature, on the nucleation and size of the WS_2 domains has been investigated. A higher nucleation temperature combined with increased substrate annealing temperatures was found to promote an increase in the WS_2 domain size. The dependence of surface coverage and coalescence behaviour of the WS_2 domains on the growth duration has also been determined, allowing monolayer WS_2 films with < 10 % bilayer to be obtained. Crystalline quality of the coalesced WS_2 films has been assessed by grazing incidence XRD and misorientation mapping using 4D-scanning transmission electron microscopy, showing a slight in-plane misorientation of the crystallites in the WS_2 monolayer. The electrical performance of the coalesced WS_2 films was assessed using backgated TLM structures demonstrating mobility values of up to 5 cm^2/Vs and a high I_{on}/I_{off} ratio greater than 10^8.

1. Introduction

A fundamental understanding of the nucleation and coalescence mechanisms of two-dimensional (2D) layers by metalorganic chemical vapor deposition (MOCVD) is of critical importance for the growth of high crystalline quality 2D materials with acceptable electrical performance suitable for industrial scale applications. Wafer-scale MOCVD growth of transition metal dichalcogenide (TMDC) layers on sapphire substrates has been demonstrated by many research groups in recent years [1–7], however, the understanding of the growth mechanisms for the optimization of the crystalline quality is still missing. One approach to obtain high crystal quality TMDC layers is unidirectional growth of nucleated crystallites that coalesce to form a layer without antiphase grain boundaries. This has been demonstrated for MOCVD of WS_2 [7] and WSe_2 [8] by optimization of nucleation, ripening and growth conditions, or for CVD growth of MoS_2 using MoO_3 and S as precursors on C-plane sapphire substrates with specific offcut (towards A-plane) [9].

Herein, we report on the preliminary study of nucleation of the

---

crystallites and coalescence behaviour of WS_2 monolayers grown by MOCVD in an AIXTRON commercial research scale close coupled showerhead (CCS®) MOCVD reactor.

The variation of growth conditions such as growth temperature, duration, as well as sapphire substrate offcut and substrate annealing conditions (temperature, carrier gas, duration) on the nucleated WS_2 crystallites size and surface coverage was investigated.

2. Materials and methods

MOCVD growth of WS_2 layers was performed in an AIXTRON CCS® 2D R&D system in a $19 \times 2''$ configuration. Tungsten hexacarbonyl (W $(CO)_6$, WCO, 94 nmol/min) was used as the tungsten (W) source and di-*tert*-butyl sulfide ($S[C(CH_3)]_2$, DTBS, 410 μmol/min) was used as the sulfur (S) source. WS_2 was deposited on sapphire substrates in a one-step continuous growth process at temperatures in the range 700–850 °C at 50 hPa reactor pressure with high S/W molar ratio of > 4000 and growth duration varying from 900 s to 3300 s. To investigate the effect of substrate miscut on the nucleation and coalescence of WS_2, C-plane (0001) sapphire substrates having different offcut angles from C-plane (0.2° towards the M−plane (C/M) and 0.25° or 1° towards the A-plane (C/A)) were used. To determine the influence of substrate preparation conditions on the crystallite nucleation and coalescence, sapphire substrates were treated with different annealing conditions: in H_2 at 1200 °C and in N_2 at 1200 °C or 1250 °C.

As-grown WS_2 domains were studied using scanning electron microscopy (SEM, Zeiss Sigma) and the domain size, as well as monolayer/bilayer coverage, were analyzed from the SEM images using a Python-based image segmentation program utilizing Otsu's thresholding concept (Supporting information Section 2). Atomic force microscopy (AFM) measurements were performed using Horiba's OmegaScope. The measurements were performed in AC tapping mode using MikroMasch Si tips with nominal radius of 8 nm and spring constant of 0.5 N/m. The coalesced WS_2 films were characterized by Raman spectroscopy (Renishaw InVia, 532 nm laser; 100x objective lens; 1800 mm^{-1} grating). WS_2 crystal quality was assessed by grazing incidence X-ray

diffraction (GIXRD) with a SmartLab Rigaku diffractometer equipped with a copper rotating anode beam tube ($K_\alpha = 1.54$ Å) operating at 45 kV and 200 mA; parallel in-plane collimators of 0.5° of resolution were used both on the source and detector sides. The diffractometer is equipped with multilayer mirrors on the incident beam side and K_β filter on the diffracted beam side; the incidence angle was set to 0.28°, close to the critical angle of the substrate (Fig. S1). The areal density of W and S of the optimized WS_2 monolayers for the estimation of layer stoichiometry was determined by Rutherford Backscattering Spectroscopy (RBS) using 2 MV tandem 6SDH Pelletron accelerator (NEC) with a He^+ ion beam with energy ranging from 500 keV to 3.5 MeV; the scattering chamber contains a 5-axis goniometer which uses a silicon surface barrier as ion beam analyzer. 4D-Scanning Transmission Electron Microscopy (4D-STEM) experiments were performed in a Titan Ultimate STEM equipped with Merlin detector, and an orientation map was generated by a custom-made script based on the template matching algorithm discussed in [10]. The electrical performance of the coalesced WS_2 films was assessed using backgated transmission line method (TLM) structures allowing extraction of both field-effect mobility as well as TLM mobility.

3. Results and discussion

A coalescence study of WS_2 films grown on 0.2° off (C/M) sapphire substrates is presented in Fig. 1 and Fig. S2. Sapphire substrates were annealed at 1200 °C for 10 min in pure H_2 atmosphere and growth was performed at 700 °C temperature. Terminating the growth process after 900 s leads to a partial sapphire coverage (<40 %) with nucleated triangular shaped WS_2 crystallites (Fig. 1a). WS_2 domains are mostly well aligned and have two main antiparallel orientations (0° and 60° domains), similar to results reported in other works on TMDC growth on sapphire [7]. With longer growth times, the domains grow in lateral size (Fig. S3a) resulting in an increased WS_2 coverage (Fig. 1b, 1c) before coalescing into a closed WS_2 film. In addition to lateral growth of WS_2 domains, second layer islands start to appear for the growth times exceeding 2000 s (i.e. at approximately 60–70 % monolayer coverage) as evidenced by additional features appearing in SEM and AFM
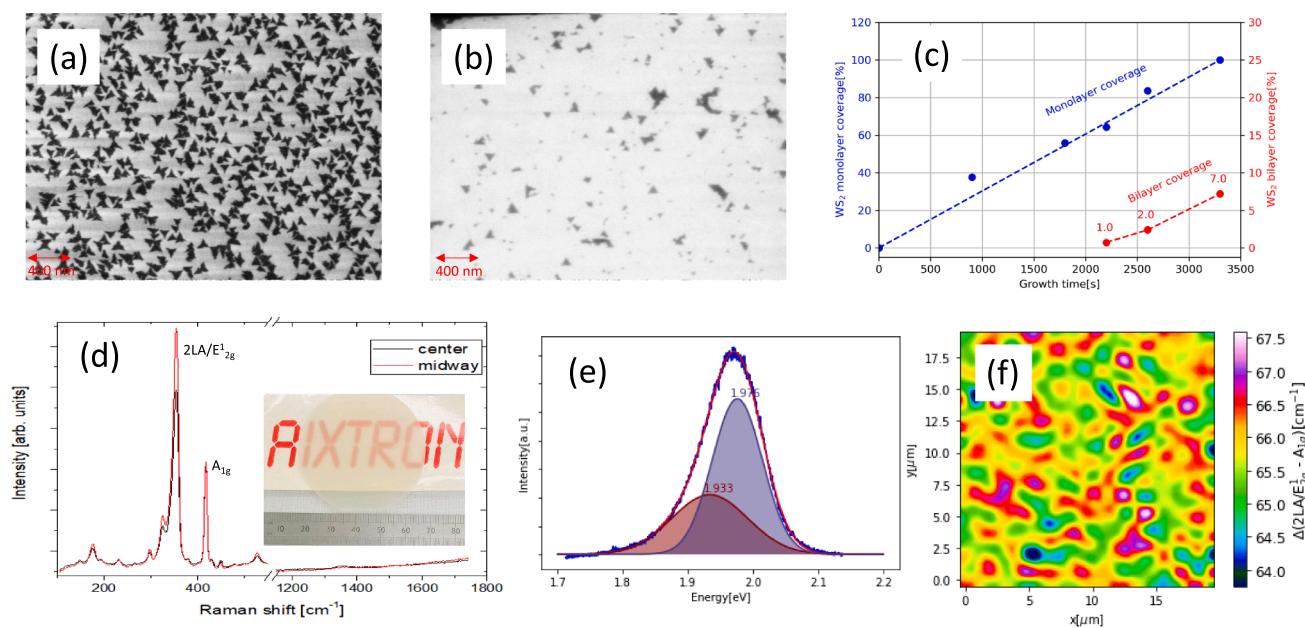

Fig. 1. WS_2 film coalescence study for growth at 700 °C on 0.2° off (C/M) sapphire: a, b) SEM image for 900 s and 3300 s growth time, respectively (Scale bar is 400 nm); c) estimated monolayer and bilayer coverage dependence on growth duration, with dashed lines illustrating the trend; d) Raman spectra of coalesced WS_2 layers at different positions on 2″ wafer; e) typical photoluminescence (PL) spectrum of a coalesced WS_2 monolayer; f) μ-Raman mapping of 2LA(M)/E^1_{2g} and A_{1g} peak difference.
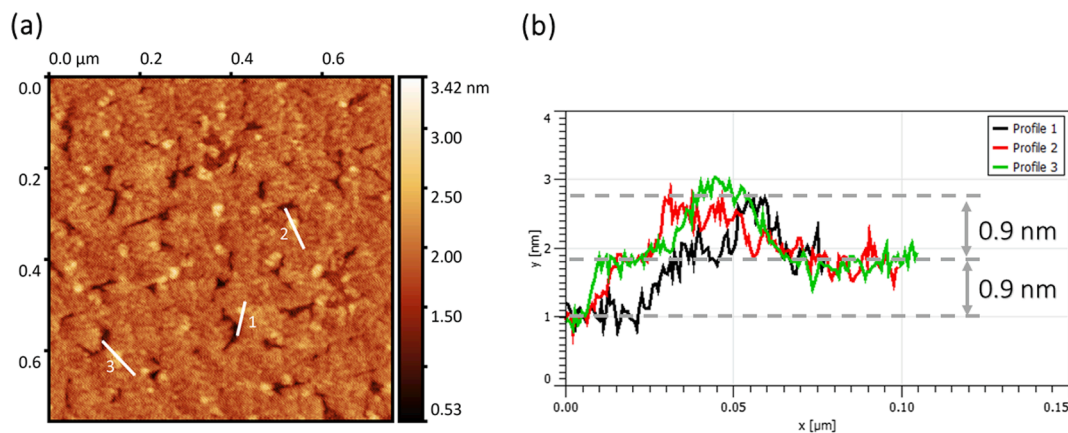
Fig. 2. (a) AFM topography micrograph of WS$_2$ film on sapphire after 2600 s growth; (b) height profiles taken at different positions indicated in (a).
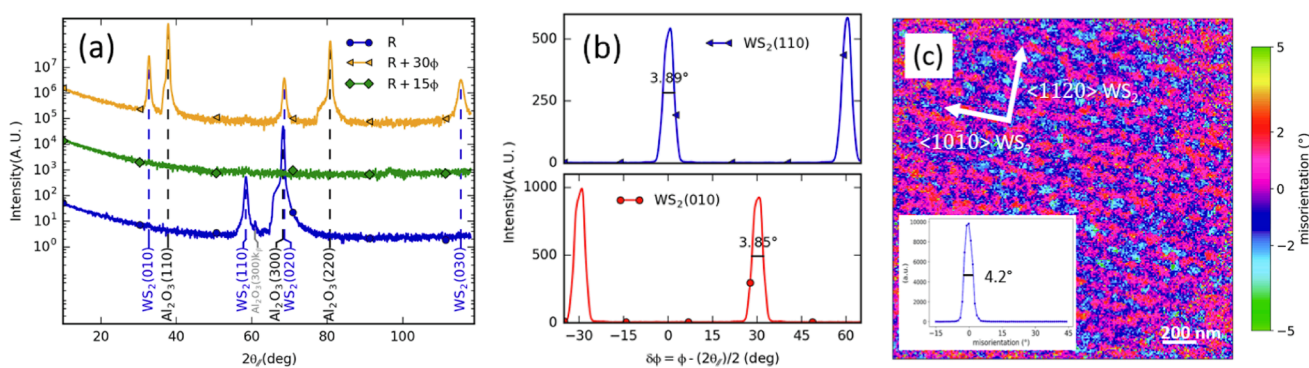

Fig. 3. a, b) GIXRD characterization of the WS$_2$ monolayer a) radial scans; b) azimuthal scans; c) in-plane misorientation map by 4D-STEM.

topography images (Fig. 2a). We estimate the WS$_2$ monolayer thickness to be approximately 0.9 nm (Fig. 2b) in line with previous reports on WS$_2$ on sapphire [7]. Both monolayer and bilayer coverage increases in an approximately linear trend until monolayer coalescence (Fig. 1c). We find a growth time of 3300 s produces a fully closed monolayer film with 7 % bi-layer.

Typical Raman spectroscopy characterisation results of coalesced films are shown in Fig. 1d. WS$_2$ Raman modes related to in-plane (2LA/E$_{2g}^1$) and out-of-plane (A$_{1g}$) vibrations are clearly distinguished (Fig. S4 a,b,c). As reported in [7], the commonly reported Raman peaks of WS$_2$ are E'(M), 2LA(M), E$_{2g}^1$(Γ), and A$_{1g}$(Γ). The difference between 2LA/E$_{2g}^1$ and A$_{1g}$ may help determining the number of layers in the WS$_2$ film on sapphire. The same Raman peak fitting is carried out as shown in Fig. S4a, with a similar distance between 2LA/E$_{2g}^1$(Γ) and A$_{1g}$(Γ) around 65.7 cm^{-1} (63.3 cm^{-1} in [7]). In addition, according to the peak position difference in a micro-Raman mapping over a 20 × 20 μm^2 area (see Fig. 1f), the variation of peak position difference is small (Δ(2LA/E$_{2g}^1$-A$_{1g}$) = 65.7 ± 1.9 cm^{-1}), indicating uniform WS$_2$ film formation in the measured area. Raman spectra are similar at different positions across the 2″ wafer indicating uniform WS$_2$ deposition and slight variations may be related to minor layer coverage variations (e.g. bilayer islands). The absence of Raman peaks in the range 1300–1600 cm^{-1} (in which D and G modes related to graphitic or amorphous carbon are expected) indicates that the degree of carbon incorporation has been minimized by optimization of the deposition process. Carbon co-deposition in MOCVD of 2D-TMDC layers is a common feature which is attributed to organic chalcogen sources used in the process; however, this may be reduced by an increased H$_2$ fraction in the carrier gas flow [11]. A typical photoluminescence spectrum of a fully coalesced WS$_2$ monolayer is presented in Fig. 1e, with the dominant PL band with peak wavelength of 620 nm

(1.995 eV) which corresponds to the intralayer exciton (typical for a WS$_2$ monolayer).

The areal density of W atoms (1.08·10^{15} at/cm^2) and S atoms (2.25·10^{15} at/cm^2) in the coalesced WS$_2$ monolayer films on 0.2° off (C/M) sapphire has been determined by RBS, resulting in a calculated layer stoichiometry (S:W ratio) of ~ 2.08, close to the theoretical stoichiometric ratio of 2 (Fig. S5).

The crystal quality and the layer orientation of monolayer WS$_2$ grown under these conditions were assessed by in-plane GIXRD measurements (Fig. S1). Both radial XRD scans (Fig. 3a) and azimuthal XRD scans (Fig. 3b) have been recorded. The full width at half maximum (FWHM) values of the WS$_2$ (1 1 0) and (0 1 0) peaks in the azimuthal scans were in the range of 3.8°-3.9°, indicating reasonable crystal quality of heteroepitaxial WS$_2$ layers grown on sapphire. In-plane misorientation of the crystallites in the WS$_2$ monolayer has been investigated by 4D-STEM mapping (Fig. S6) on a representative sample area of 4 μm^2 (Fig. 3c). A stripe-like pattern with characteristic length of about 45 nm (equivalent to a miscut of 0.27°, which is within the specifications of nominal sapphire miscut value of 0.2° ± 0.1°) is visible in the orientation map of WS$_2$ suggesting a step-edge-guided nucleation of WS$_2$ on sapphire terraces. Moreover, a slight misorientation of the crystallites (FWHM 4.2°, inset of Fig. 3c) has been detected that correlates well with the width of the azimuthal XRD peaks performed on the wafer scale sample.

The electrical properties of the coalesced WS$_2$ layers have been assessed from backgated TLM device structures displayed in an optical microscope image in Fig. 4a. These structures allow to estimate both field-effect and TLM mobility. For electrical evaluation the WS$_2$ layers are transferred from the sapphire growth template to a 50 nm SiO$_2$/Si target coupon employing a PMMA/TRT based manual transfer
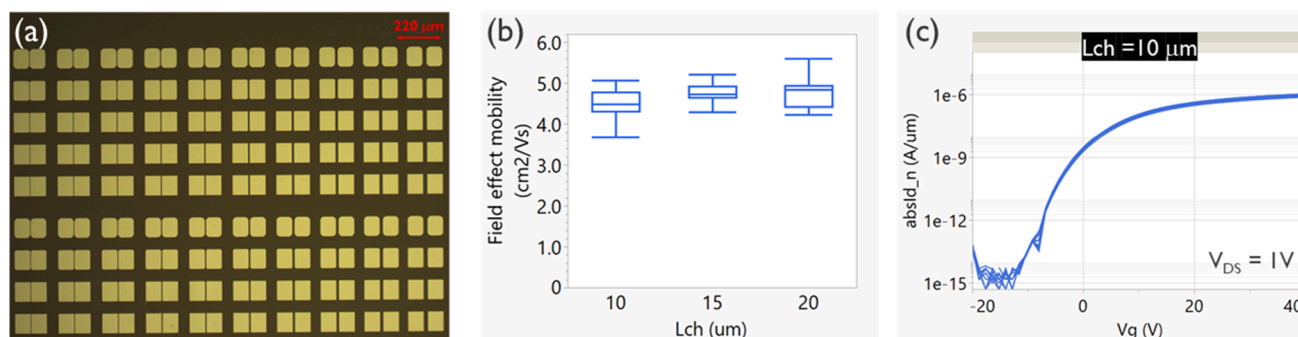
Fig. 4. Electrical characterization of monolayer WS$_2$ films: a) micrograph of TLM structure; b) estimated field-effect mobility for different channel lengths; c) drain current for different gate voltages V$_g$.
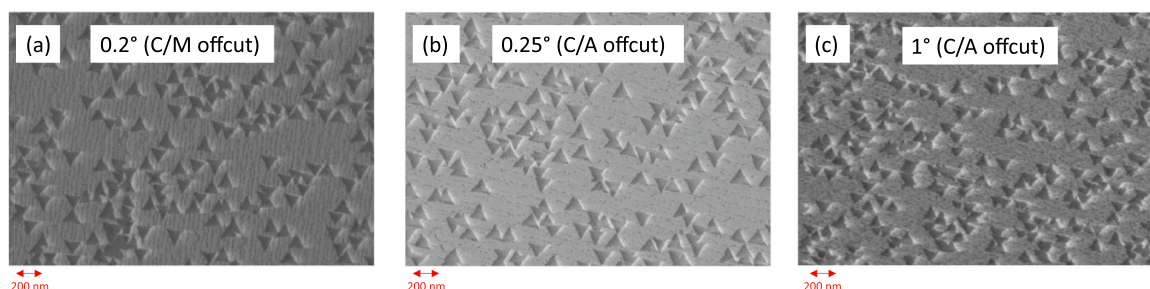

Fig. 5. WS$_2$ domains at higher growth temperature 850 °C on varying offcut sapphire annealed at 1250 °C/N$_2$: a) 0.2° off (C/M); b) 0.25° off (C/A); c) 1° off (C/A).
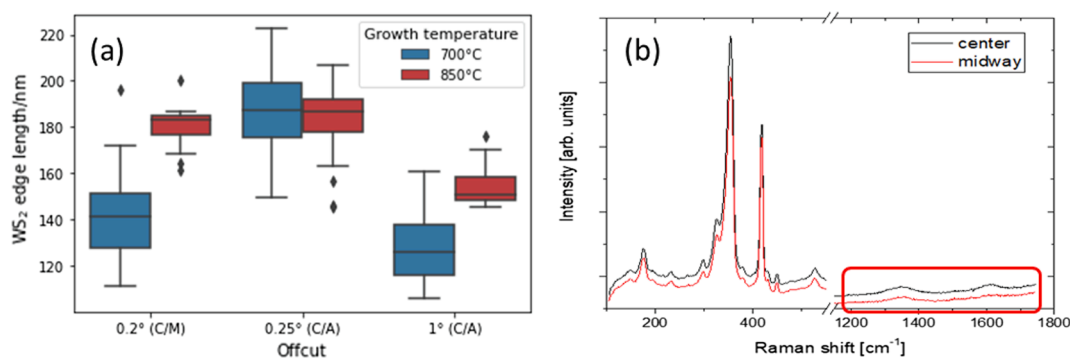

Fig. 6. a) WS$_2$ edge length on sapphire substrates with various offcuts and b) Raman spectra of WS$_2$ layers on 0.2° (C/M) sapphire (carbon signatures marked).

technique. Basic 2PP- electrical devices, with only minimal process impact, are obtained with a single litho print by e-beam lithography. Contact metals are deposited by evaporation, using a Ni/Pd stack for contact metal, and the device is finalized by lift-off. To avoid impact from a channel patterning process, mechanical channel isolation is performed [12]. TLM test structures are obtained with channel lengths (L$_{ch}$) ranging from 0.5 μm to 20 μm, while the channel width (W) is kept constant at 100 μm. In Fig. 4b, 2PP-field-effect mobility extraction is done for selected channel lengths. For long channels, these values of $\sim$ 5 cm^2/Vs overlap with TLM mobility extracted, identifying the contact resistance not to be a dominant factor in the device performance. Moreover, high I$_{on}$/I$_{off}$ ratios > 10^8 (Fig. 4c) were obtained for the WS$_2$ monolayers with only small variations over the coupon.

For further improvement of crystal quality, different sapphire substrate offcuts and orientations were considered, as the C/A offcut of sapphire substrates has previously been reported to promote unidirectional growth of MoS$_2$ crystallites [9]. Also, it has been published that a certain offcut of the sapphire is needed to obtain uniform electrical results across the wafer [12]. By using similar process conditions (700 °C and 900 s growth duration) as for C/M substrates, no unidirectional WS$_2$

domain orientation was observed on C/A sapphire (Fig. S7), however, in both cases, two preferential antiparallel (180° rotated) orientations of the crystallites were present. Significantly higher crystallite sizes were found (up to 190 nm edge length) when growing on 0.25° (C/A) sapphire, as compared to 140 nm edge length on C/M sapphire with similar offcut angle (Fig. 5 and Fig. 6a, blue boxplots). This indicates that substrate offcut orientation is indeed an important parameter affecting the WS$_2$ nucleation processes. A low value of C/A offcut promotes the formation of slightly wider sapphire terraces (as visible in Fig. S7), which may promote surface diffusion thus resulting in larger crystal domains. However, increasing the offcut value to 1° reduces the terraces width, again resulting in smaller domain sizes.

We speculate that higher growth temperatures are needed to further promote adatom surface diffusion in order to achieve an expected step-edge-guided growth mode with preferential WS$_2$ orientation (e.g. observed for MoS$_2$ in [13]). An increase of growth temperature to 850 °C leads to more pronounced triangular shapes of WS$_2$ crystallites (Fig. 5) and to larger domain sizes (Fig. 6a, red boxplots). The triangular WS$_2$ domains on the 0.2° (C/M) offcut sapphire are generally oriented perpendicular to the sapphire terraces formed by the substrate annealing

step, whereas the domains on the 0.25° (C/A) offcut sapphire are oriented parallel to the terraces. This means the substrate offcut orientation may be an instrument to control the terraces and domain growth. However, in both cases, antiphase triangular domains (rotated mutually by 180°) are present in approximately equal ratio, in disagreement with [13] for MoS_2 grown on 0.25° off (C-A) offcut sapphire.

In addition to higher growth temperature, sapphire pre-anneal conditions were also somewhat different (1250 °C in N_2), therefore the differences observed in the present study cannot be fully attributed to the higher growth temperature. The increase in temperature, however, had no clear effect on crystallite orientation (again no unidirectional crystallites were obtained, however clear two antiparallel orientations are observed (antiphase domains)). Further increase in temperature was not considered in this work, as with current conditions, significant carbon incorporation into WS_2 films grown at 850 °C was already observed by Raman spectroscopy (Fig. 6b).

4. Conclusions

An AIXTRON research scale MOCVD reactor has been successfully applied for the heteroepitaxial growth of WS_2 layers. The coalescence point of nucleated WS_2 domains was found by an almost linear increase of surface coverage with growth duration. The obtained monolayer WS_2 had preferential orientation according to the in-plane GIXRD measurements: the films (FWHM values of the WS_2 (1 1 0) and (0 1 0) peaks in the azimuthal scans were 3.8°-3.9°), indicating reasonable crystal quality of heteroepitaxial WS_2 layers. A slight in-plane local misorientation of the crystallites in a continuous WS_2 layer has been detected by 4D-STEM with an angle distribution of 4.2° (FWHM). RBS measurements show the grown WS_2 layers to be stoichiometric, with S:W ratio ~ 2.08, and reasonable electrical properties (field-effect and TLM mobility ~ 5 cm^2/Vs with high I_{on}/I_{off} ratios > 10^8) were obtained for the WS_2/sapphire layers grown under optimized conditions. Finally, sapphire substrate offcut angle and orientation as well as growth temperature were shown to significantly impact initial stages of WS_2 growth. Thus, understanding and controlling crystallite nucleation and coalescence by substrate surface preparation as well as different growth conditions are essential in further improving crystalline quality of TMDC films grown by MOCVD.

CRediT authorship contribution statement

Haonan Tang: Software, Investigation, Writing – original draft, Writing – review & editing. **Sergej Pasko:** Investigation, Writing – original draft, Writing – review & editing. **Simonas Krotkus:** Investigation, Writing – original draft, Writing – review & editing. **Thorsten Anders:** Project administration. **Cornelia Wockel:** Investigation. **Jan Mischke:** Investigation, Writing - review & editing. **Xiaochen Wang:** Investigation. **Ben Conran:** Investigation. **Clifford McAleese:** Methodology. **Ken Teo:** Funding acquisition. **Sreetama Banerjee:** Investigation. **Henry Medina Silva:** Investigation. **Pierre Morin:** Investigation. **Inge Asselberghs:** Resources. **Amir Ghiami:** Investigation. **Annika Grundmann:** Methodology. **Songyao Tang:** Investigation. **Hleb Fiadziushkin:** Investigation. **Holger Kalisch:** Investigation, Methodology. **Andrei Vescan:** Resources. **Salim El Kazzi:** Conceptualization. **Alain Marty:** Investigation. **Djordje Dosenovic:** Investigation. **Hanako Okuno:** Investigation. **Lucie Le Van-Jodin:** Project administration. **Michael Heuken:** Supervision, Conceptualization, Resources, Funding acquisition, Writing – review & editing.

Declaration of Competing Interest

The authors declare that they have no known competing financial interests or personal relationships that could have appeared to influence the work reported in this paper.

Data availability

Data will be made available on request.

Acknowledgements

Appendix A. Supplementary material

Supplementary data to this article can be found online at https://doi.org/10.1016/j.jcrysgro.2023.127111.

References

[1] M. Marx, et al., J. Cryst. Growth 464 (2017) 100–104.
[2] (a) M. Heuken, et al., Proc. SPIE (2019) 10940;
(b) M. Heuken, et al., Meet. Abstr. MA2021-02 (2017) 606.
[3] A. Grundmann, et al., MRS Adv. 5 (31–32) (2020) 1625–1633.
[4] D. Andrzejewski, et al., ACS Photon. 6 (8) (2019) 1832–1839.
[5] S. Tang, et al., MRS Adv. 7 (30) (2022) 751–756.
[6] A. Cohen, et al., ACS Nano 15 (1) (2021) 526–538.
[7] M. Chubarov, et al., ACS Nano 15 (2) (2021) 2532–2541.
[8] X. Chen, et al., Appl. Surf. Sci. 567 (2021), 150798.
[9] T. Li, et al., Nature Nanotech. 16 (2021) 1201–1207.
[10] E. Rauch, et al., Z. Kristallogr. 225 (2-3) (2010) 103–109.
[11] Ch.M. Schaefer, et al., Chem. Mater. 33 (12) (2021) 4474–4487.
[12] Y. Shi, et al., ACS Nano 15 (6) (2021) 9482–9494.
[13] J. Mo, et al., Nanotechnology 31 (2020), 125604.